journal

J. Am. Ceram. Soc., 99 [8] 2752–2759 (2016)
DOI: 10.1111/jace.14268

Thermodynamic Stability of Low-*k* Amorphous SiOCH Dielectric Films

Jiewei Chen,[‡] Sean W. King,[§] Elayaraja Muthuswamy,[‡] Anastasia Koryttseva,[‡,¶] Di Wu,[‡] and Alexandra Navrotsky[‡,†]

[‡]Peter A. Rock Thermochemistry Laboratory and NEAT ORU, University of California Davis, Davis, California 95616

[§]Logic Technology Development, Intel Corporation, Hillsboro, Oregon 97124

[¶]Department of Chemistry, N.I. Lobachevsky State University of Nizhny Novgorod, 23 Gagarin Avenue, Nizhny Novgorod 603950, Russia

Si–O–C-based amorphous or nanostructured materials are now relatively common and of interest for numerous electronic, optical, thermal, mechanical, nuclear, and biomedical applications. Using plasma-enhanced chemical vapor deposition (PECVD), hydrogen atoms are incorporated into the system to form SiOCH dielectric films with very low dielectric constants (*k*). While these low-*k* dielectrics exhibit chemical stability as deposited, they tend to lose hydrogen and carbon (as labile organic groups) and convert to SiO_2 during thermal annealing and other fabrication processes. Therefore, knowledge of their thermodynamic properties is essential for understanding the conditions under which they can be stable. High-temperature oxidative drop solution calorimetry measurement in molten sodium molybdate solvent at 800°C showed that these materials possess negative formation enthalpies from their crystalline constituents (SiC, SiO_2, C, Si) and H_2. The formation enthalpies at room temperature become less exothermic with increasing carbon content and more exothermic with increasing hydrogen content. Fourier transform infrared spectroscopy (FTIR) spectroscopy examined the structure from a microscopic perspective. Different from polymer-derived ceramics with similar composition, these low-*k* dielectrics are mainly comprised of Si–O(C)–Si networks, and the primary configuration of carbon is methyl groups. The thermodynamic data, together with the structural analysis suggest that the conversion of sp^2 carbon in the matrix to surface organic functional groups by incorporating hydrogen increases thermodynamic stability. However, the energetic stabilization by hydrogen incorporation is not enough to offset the large entropy gain upon hydrogen release, so hydrogen loss during processing at higher temperatures must be managed by kinetic rather than thermodynamic strategies.

Keywords: *amorphous low-k SiOCH films; formation enthalpy; thermodynamic stability*

I. Introduction

The silicon–oxygen–carbon system includes a variety of materials of technological and scientific importance.[1] However, there are currently no known thermodynamically stable crystalline compounds comprising of all three elements in the Si–O–C system.[1,2] In contrast, amorphous materials that combine all three components are relatively common and of interest for numerous electronic,[3] optical,[4] thermal,[5] mechanical,[6] nuclear,[7] and biomedical[8] applications. Glassy SiOC materials are in particular desired as replacements for traditional SiO_2-based glasses due to low dielectric constant,[9] high-temperature stability,[10] and enhanced thermal, mechanical, and chemical properties.[11] The crystallization resistance of SiOC materials has been attributed to kinetic factors related to slow long-range diffusion of silica. In 2007, Varga *et al.* for the first time demonstrated that the good thermal stability may arise from thermodynamic as well as kinetic factors.[12] Results showed that these glassy SiOC ceramics synthesized from polymer precursors exhibited a negative enthalpy of formation from a mixture of SiC, SiO_2, and C, perhaps related to the presence of mixed bonds at the interface of the nanodomains in the structure. Since these materials are strongly disordered, their entropy of formation from crystalline components is expected to be positive, and their free energy of formation even more negative than their enthalpy of formation.

Recently, some stable Si–O–C materials have been synthesized containing the addition of a fourth element—hydrogen.[13,14] One route involves chemical vapor deposition (CVD)[15] or plasma-enhanced CVD (PECVD)[16,17] to make thin film SiOCH materials using various organosilane or alkoxysilane precursors in combination with strong or weak oxidizers such as O_2, N_2O, and CO_2.[18] Currently, the PECVD method has been widely adopted within the semiconductor industry for depositing amorphous SiOCH (a-SiOCH) materials with values of dielectric permittivity that are substantially reduced relative to SiO_2.[14,16] Such "low-*k*" dielectric materials are of vital importance to the semiconductor industry for reducing parasitic capacitive signal delays and power loss in highly scaled and integrated micro and nano-electronic products.[19]

While low-*k* dielectrics exhibit clear chemical stability as deposited, they have a great propensity to lose hydrogen and carbon (as labile organic groups) and convert to SiO_2 during thermal annealing and other nano-electronic acid/base wet chemical cleaning and plasma etching fabrication processes.[20–23] This calls into question the general thermodynamic stability of low-*k* materials and their interfaces with other materials as well as the long-term reliability of products manufactured from them.[24,25] However, basic thermodynamic data such as the enthalpy and entropy of formation are completely lacking these and related materials. Thus, there is a great need to understand the thermochemistry of low-*k* a-SiOCH materials to assess their ultimate stability in highly scaled and integrated nano-electronic products. Examination of the thermochemistry of low-*k* a-SiOCH materials will also broaden the understanding of the energy landscape in the Si–O–C and Si–O–C–H systems.[12,26–29]

In this context, we studied the thermochemistry for a series of low-*k* dielectric a-SiOCH thin films synthesized by PECVD. We measured the heat of oxidative dissolution of these PECVD synthesized low-*k* a-SiOCH materials in

R. Riedel—contributing editor

Manuscript No. 37927. Received December 29, 2015; approved March 21, 2016.
[†]Author to whom correspondence should be addressed. e-mail: anavrotsky@ucdavis.edu

molten sodium molybdate at 800°C, from which the oxidation and formation enthalpies at room temperature were calculated. The enthalpy data clearly show that the addition of hydrogen stabilizes the SiOC materials.

II. Experimental Methods

(1) Sample Preparation

The a-SiOCH materials were deposited on 300 mm diameter Si (001) wafers by PECVD using either an organosilane or alkoxsilane in combination with various diluent (H_2, He) and/or oxidizing gases (O_2, CO_2) at temperatures ranging from 250°C–400°C.[30,31] In some cases, a phenyl-based organic precursor was added to the PECVD chemistry and incorporated into the film as a second phase material and then removed from the matrix postdeposition using a ~400°C ultraviolet cure.[32] The full elemental composition of the SiOCH films was determined via combined Rutherford backscattering and nuclear analysis (RBS-NRA) measurements performed at the SUNY Albany Dynamitron Accelerator Laboratory. The details of synthesis and characterization have been described previously.[18,32–34] The compositions and electrical properties of these films are listed in Table I.

After deposition, the films were removed from the substrate to form 20–200 mg of powder via two different methods. For the highest hydrogen content films, the adhesion to the substrate was sufficiently low that the films could be easily scraped off manually using a razor blade. For the lower hydrogen content films, the adhesion was too high for this method to be practical. To form powders, these films were deposited on Cu due to the reduced adhesion energy,[35] so that they could be easily removed from the substrate.

(2) Powder X-ray Diffraction

All samples were characterized by powder X-ray diffraction (PXRD) on a Bruker D8 (Madison, WI) (AXS) Advance diffractometer using Cu$K\alpha$ radiation (40 kV, 40 mA). The scans were acquired in the 2θ range of 10°–95° with a step size of 0.02° using a low-background quartz holder.

(3) Fourier Transform Infrared (FTIR) Spectroscopy

To examine the chemical structure of the materials, thinner films (500 nm) were deposited on Si (001) substrates and examined using transmission Fourier transform infrared (FTIR) spectroscopy. Spectra were collected using both Nicolet Magna-IR 860 and Bio-Rad QS-3300 spectrometers.[33] Normal incidence IR transmission spectra of samples on Si substrate samples were collected using an open beam background. All spectra were acquired from 400 to 7000 cm^{-1} with 4 cm^{-1} resolution and signal averaged over 128 scans. The spectrum of the Si substrate was obtained by prescanning it prior to deposition. This spectrum was utilized for removing the Si substrate absorption from the sample spectrum as well as correcting for optical interference effects common in transmission measurements of thin films on thick substrates.[36] The latter corrections used rigorous methods that account for the full wave nature of light and have been previously described in detail.[36,37]

(4) Calorimetry

High-temperature oxidative drop solution calorimetry was utilized to determine the oxidation and formation enthalpies of the films. Similar compounds have been studied previously by the same technique in our laboratory and we used the experimental method described by Tavakoli *et al.*[28] In a typical measurement, 0.75–1.5 mg pellets were dropped from room temperature into molten sodium molybdate ($3Na_2O{\cdot}4MoO_3$) solvent maintained at 800°C inside an AlexSYS Setaram isoperibol Tian-Calvet twin microcalorimeter (Setaram Instruments, Cailune, France). Oxygen gas was bubbled through the solvent (~5 mL/min) to enhance oxidation and stir the melt. The oxidation of the samples resulted in the formation of gaseous products (CO_2, H_2O) which were removed immediately by continuous flushing of oxygen gas (~25 mL/min) through the calorimeter assembly. The calorimeter was calibrated against the heat content of platinum pellets. Statistically reliable data (within 2% error) were obtained by dropping a number of pellets. This methodology is well-established[38–40] and similar to that in recent studies.[28]

III. Results and Discussion

(1) XRD Analysis

The PXRD patterns confirmed the amorphous nature of these SiOCH samples. Two samples (#1, #2) were completely amorphous (Fig. 1), whereas the rest of the samples (#3, #4, #5) showed the existence of crystalline impurities (Fig. 2). As mentioned above, these three samples had been deposited on a copper substrate. The copper impurity presumably entered the sample when it was scraped off the substrate. Based on the intensities of the reflections in Figs. 1 and 2 and copper being a strong diffractor, it was estimated that the amount of copper in these samples was certainly <10% and probably less than 5%. A calculation (see Appendix II) showed that its effect on the drop solution enthalpy was well below the experimental uncertainty in the measurements.

(2) FTIR

Figures 3 and 4 present FTIR spectra of the five materials examined in this study. Figure 3 focuses on the 500–1500 cm^{-1} window that encompasses the Si–C (ν Si–C) and Si–O–Si asymmetric stretching (ν^a Si–O–Si) modes and Fig. 4 focuses on the 1800–3400 cm^{-1} window that encompasses the Si–H (ν Si–H) and C–H (ν C–H) stretching modes. For the a-SiCH film (#4) with limited amount of oxygen, only the Si–C stretching mode at ~760 cm^{-1} was observed.[33] For other SiOCH films, both the Si–C and Si–O stretching modes at ~810 and 1060 cm^{-1} were observed, indicating that the network structure for these materials consists of both Si–C–Si and Si–O–Si linkages. The absorption band centered at 800 cm^{-1}exhibits several clear subcomponents that are attributed to $SiC–H_3$-related rocking modes (i.e., ρ $SiCH_3$).[41] This indicates that the Si–C network bonding in these materials

Table I. Compositional Information and Properties of Low-*k* a-SiOCH Films

Sample #	Film type	Precursor†	Si‡	O‡	C‡	H‡	Powder color-type	*k*
1	a-SiOCH	AOS#1	16.4	26.1	15	42.5	Fine white powder	3.3
2	a-SiOCH	AOS#4	18.5	25.6	17.7	38.3	Fine tan powder	3.05
3	a-SiCOH	OS#3	25.4	19.6	22.6	32.5	Clear thin film flakes	4.8
4	a-SiCH	OS#3	37.1	0.3	36.3	26.3	Amber color thin film flakes	7.2
5	a-SiOCH	OS#3	36.1	45.2	10	8.6	Amber color thin film flakes	4.2

†AOS stands for precursor alkoxysilanes; OS means organosilanes.
‡The composition is presented in atomic percentage.

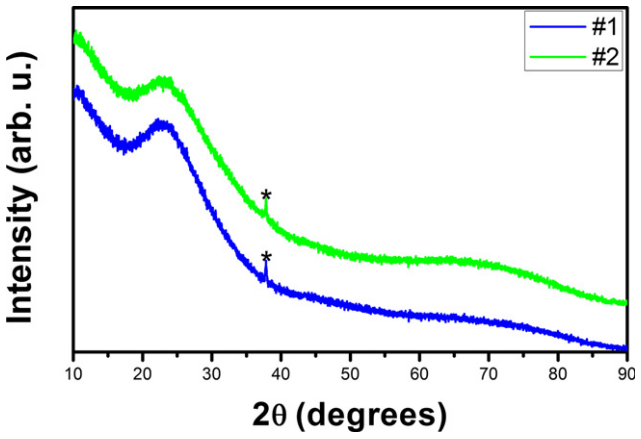

Fig. 1. Powder X-ray diffraction (PXRD) patterns of low-*k* a-SiOCH samples (#1, #2). The peak marked with a star represents the reflection from XRD holder.

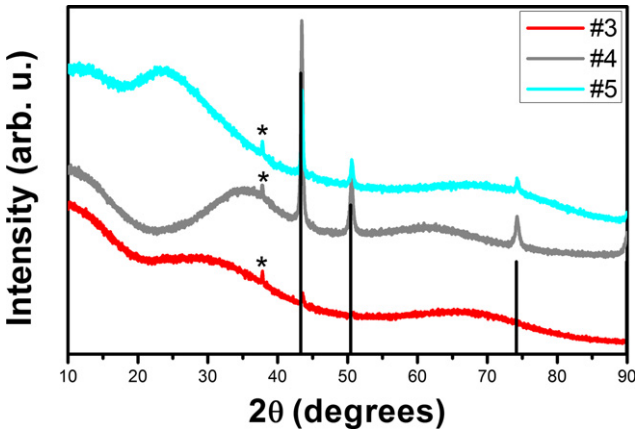

Fig. 2. PXRD patterns of low-*k* a-SiOCH samples (#3, # 4, #5) compared to the copper reference pattern (ICDD PDF card # 04-0836). The peak marked with a star represents the reflection from XRD holder.

has been interrupted/replaced by terminal methyl (CH_3) groups. The presence of terminal CH_3 groups is confirmed by an additional absorption band at 1250–1270 cm^{-1} that has been attributed to the SiC–H_3 symmetric deformation mode (δ^s SiC–H_3).[41] Evidence for Si–H bonding is also shown in Fig. 3 by the Si–H deformation band (δ Si–H) at 890 cm^{-1}.[41]

The C–H stretching mode shown in Fig. 4 also supports the assignment of the absorption bands at ~800 and 1270 cm^{-1} in the two a-SiOCH films (#1, #2) to SiC–H_3 rocking and deformation bands, respectively. Specifically, the C–H stretching band in these two films show clear peaks in absorbance at 2960 and 2920 cm^{-1} that can be attributed to asymmetric and symmetric stretching modes of terminal CH_3 groups.[41] More detailed examination of the C–H absorption band for these two films also shows peaks at 2940 and 2880 cm^{-1} that indicate the presence of some methylene groups (CH_2) in the structure of these materials. For the other three materials, the C–H stretching band appears only as a single broad absorption band centered at progressively lower wave numbers. The broad nature indicates the presence of a mix of CH_1, CH_2, and CH_3 entities. The progressively lower wave number position for the C–H stretching mode as the carbon concentration increases is also consistent with the back-bonding changing from primarily O_3–Si to C_3–Si similar to what has been previously discussed for the Si–H stretching mode.[42,43]

In summary, FTIR spectra show that the structure of these SiOCH materials is mainly comprised of Si–O–Si and Si–C–Si networks, whereas for oxygen-poor SiCH films,

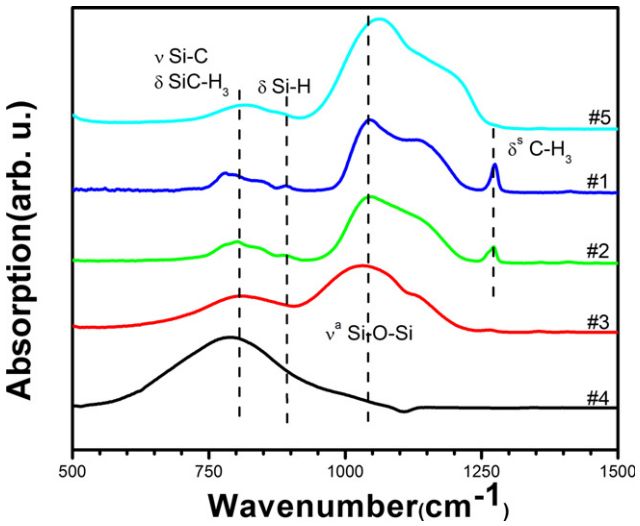

Fig. 3. FTIR spectra of low-*k* a-SiOCH materials in the window of 500–1500 cm^{-1}.

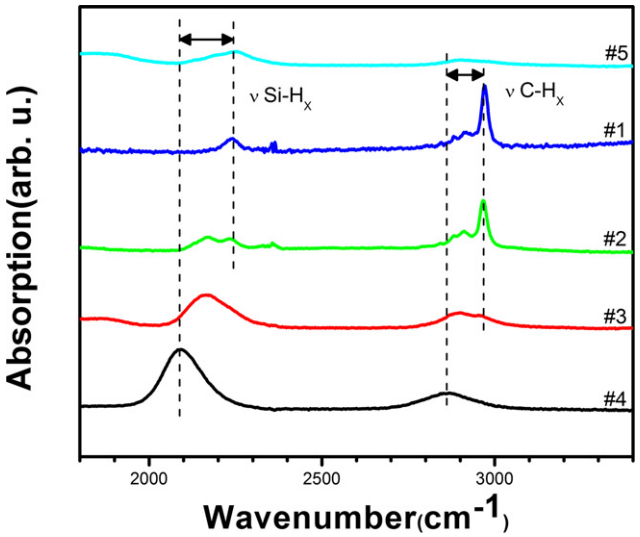

Fig. 4. FTIR spectra of low-*k* a-SiOCH materials in the window of 1800–3400 cm^{-1}.

there is limited amount of Si–O–Si presented in the structure. The primary configurations of carbon atoms are bridging bonds between Si atoms and methyl groups. Evidence of carbon–carbon bonds in the spectra was absent due to the lack of any detectable absorption at 1600 cm^{-1} attributable to sp^2 C=C bonding. The incorporation of hydrogen atoms causes the transformation from Si–C–Si to –CH_3 for carbon atoms. Grill *et al.* provided a similar structure model based on a careful FTIR characterization.[44] It is notable that the structure of SiOCH films synthesized by PECVD is quite different from that of SiOCH synthesized from pyrolysis of a polymer under H_2 atmosphere. In polymer-derived SiOCH, there is clear separation between two nano phase regions—amorphous silica-rich domains with many Si–O–Si bonds similar to the bonds in SiO_2 and graphene sheet domains with sp^2 carbon atoms bonded to each other. Mixed-bond tetrahedra of type $SiO_{4-n}C_n$, where $n = 1$, 2, or 3, link these two regions.[12,26,45,46]

(3) High-Temperature Oxide Melt Solution Calorimetry

The calorimetric measurements obtained the enthalpy of oxidation and of formation of a-SiOCH films with respect to elements, as well as to a mechanical mixture of crystalline

SiC, SiO_2, C(Si), and H_2 at 25°C. The high-temperature oxide melt drop solution enthalpies were obtained directly from experiments, see Table II. The drop solution experiment measures the enthalpy ΔH_{ds} of the reaction:

$$\mathrm{Si}_a\mathrm{O}_b\mathrm{C}_c\mathrm{H}_d\ (\mathrm{solid}, 25°\mathrm{C}) + \left(a + c + \frac{d}{4} - \frac{b}{2}\right)\mathrm{O}_2\ (\mathrm{gas}, 802°\mathrm{C}) \rightarrow a\mathrm{SiO}_2\ (\mathrm{cristobalite}, 802°\mathrm{C}) + c\mathrm{CO}_2\ (\mathrm{gas}, 802°\mathrm{C}) + \frac{d}{2}\mathrm{H}_2\mathrm{O}\ (\mathrm{gas}, 802°\mathrm{C}) \quad (1)$$

The rationale and evidence for these final states are discussed elsewhere.[12] The room-temperature oxidation enthalpies and formation enthalpies were then determined by the thermodynamic cycles shown in the Appendix I. The oxidation enthalpies at room temperature refer to the reaction

$$\mathrm{Si}_a\mathrm{O}_b\mathrm{C}_c\mathrm{H}_d\ (\mathrm{solid}, 25°\mathrm{C}) + \left(a + c + \frac{d}{4} - \frac{b}{2}\right)\mathrm{O}_2\ (\mathrm{gas}, 25°\mathrm{C}) \rightarrow a\mathrm{SiO}_2\ (\mathrm{cristobalite}, 25°\mathrm{C}) + c\mathrm{CO}_2\ (\mathrm{gas}, 25°\mathrm{C}) + \frac{d}{2}\mathrm{H}_2\mathrm{O}\ (\mathrm{gas}, 25°\mathrm{C}) \quad (2)$$

Results are listed in Table II. All the oxidation enthalpies are strongly exothermic, and although the entropy of oxidation is negative because gas is consumed, the Gibbs free energies of oxidation are expected to remain negative. Thus, these films are metastable in atmospheres containing oxygen, but the kinetics of oxidation is slow, and oxidation in air probably does not set in below 600°C.[47]

The enthalpies of formation from the elements, calculated from the thermodynamic cycles in Appendix I, are also strongly negative, see Table II. The leading term in these enthalpies is the strongly negative heat of formation of silica. Thus, the films are clearly stable with respect to their elemental constituents.

Of particular interest is the enthalpy of formation of the amorphous films from the constituent crystalline SiO_2, SiC, C, (Si), and gaseous H_2. This formation reaction can be written as

$$\left(a - \frac{b}{2}\right)\mathrm{SiC}\ (\mathrm{solid}, 25°\mathrm{C}) + \frac{b}{2}\mathrm{SiO}_2\ (\mathrm{cristobalite}, 25°\mathrm{C}) + \left(c - a + \frac{b}{2}\right)\mathrm{C}\ (\mathrm{solid}, 25°\mathrm{C}) + \frac{d}{2}\mathrm{H}_2\ (\mathrm{gas}, 25°\mathrm{C}) \rightarrow \mathrm{Si}_a\mathrm{O}_b\mathrm{C}_c\mathrm{H}_d\ (\mathrm{amorphous\ solid}, 25°\mathrm{C}) \quad (3-a)$$

Or, in cases where free silicon appears to be required by stoichiometry

$$c\mathrm{SiC}\ (\mathrm{solid}, 25°\mathrm{C}) + \frac{b}{2}\mathrm{SiO}_2\ (\mathrm{cristobalite}, 25°\mathrm{C}) + \left(a - c - \frac{b}{2}\right)\mathrm{Si}\ (\mathrm{solid}, 25°\mathrm{C}) + \frac{d}{2}H_2\ (\mathrm{gas}, 25°\mathrm{C}) \rightarrow \mathrm{Si}_a\mathrm{O}_b\mathrm{C}_c\mathrm{H}_d\ (\mathrm{solid}, 25°\mathrm{C}) \quad (3\text{-}b)$$

Values are summarized in Table II. All these enthalpies are negative. Since the entropies of formation of the amorphous and disordered films are expected to be positive, their Gibbs free energies are even more negative than their enthalpies, implying that the films are thermodynamically stable with respect to crystalline components. This thermodynamic stability parallels that of the polymer-derived ceramics studied earlier,[12,26,28,29] but the incorporation of hydrogen appears to lead to even more negative enthalpies, as was already seen for the nanopowders studied by Tavakoli.[29]

The structure and bonding of a material on the atomic, nano- and microscales on one hand can be reflected from thermodynamic properties from a macroscopic perspective. On the other hand, the thermodynamic data directly obtained from experiments can be in turn be explained by the structure, such as the number, type, and strength of chemical bonds and the short-, mid- and long-range order in the material.

To document the relations between the enthalpies and structural information, room-temperature oxidation enthalpies and formation enthalpies from elements are plotted with respect to the carbon and hydrogen content (Fig. 5). From Fig. 5(a), we can see that the formation enthalpies are strongly exothermic, and become less exothermic as carbon content increases, indicating lower thermodynamic stability with higher carbon concentration. Similar conclusions can be drawn from the oxidation enthalpies. They are strongly exothermic, being dominated by the oxidation of carbon, supported by the observation that they become more negative with increasing carbon content.

According to our FTIR analysis, in these a-SiOCH films, carbon atoms exist in the form of $–CH_3$ groups bonded to Si as terminal groups, as well as in the form of Si–C–Si bridges. The amount of carbon with sp^2 structure is below the detection limit. ^{13}C solid-state nuclear magnetic resonance by Mabboux *et al.* also supports the conclusion that methyl groups are the main configuration and no sp^2-bonded carbon can be detected in PECVD-synthesized SiOCH films.[48] From thermodynamic analysis, the presence of carbon in other forms such as sp^2 carbon rather than carbon in the form of methyl groups would diminish thermodynamic stability, or conversely the conversion of sp^2 carbon to methyl groups by incorporating hydrogen would increase thermodynamic stability. Moreover, our conclusion is also supported by Tavakoli *et al.*, who concluded that the free carbon did not provide additional thermodynamic stability to the polymer-

Table II. Enthalpies of Drop Solution (ΔH_{ds}), Enthalpies of Oxidation at Room Temperature (ΔH^0_{ox}, 25°C), Enthalpies of Formation from Elements ($\Delta H^0_{f,elem}$), Enthalpies of Formation ($\Delta H^0_{f,comp}$) from Compounds for Different a-SiOCH Compositions

Sample #	Composition¶ Si	O	C	H	ΔH_{ds} [kJ·(g·at.)$^{-1}$]	ΔH^0_{ox} [kJ·(g·at.)$^{-1}$]	$\Delta H^0_{f,elem}$ [kJ·(g·at.)$^{-1}$]	$\Delta H^0_{f,comp}$ [kJ·(g·at.)$^{-1}$]
4	37.1	0.3	36.3	26.3	−458.32 ± 5.80(7)†	−479.94 ± 5.80	−37.50 ± 6.17	−9.57 ± 9.06‡
3	25.4	19.6	22.6	32.5	−211.04 ± 2.79(8)	−232.41 ± 2.79	−133.71 ± 3.49	−33.27 ± 7.50§
2	18.5	25.6	17.7	38.3	−149.95 ± 1.21(8)	−171.51 ± 1.21	−120.92 ± 2.43	−0.47 ± 7.07§
1	16.4	26.1	15.0	42.5	−101.71 ± 1.45(8)	−123.76 ± 1.45	−144.98 ± 2.56	−23.98 ± 7.12§
5	36.1	45.2	10	8.6	−94.68 ± 0.70(8)	−113.17 ± 0.70	−266.47 ± 2.20	−53.85 ± 7.00‡

†Uncertainty is two standard deviations of the mean. The number in the parentheses is the number of experiments.
‡$\Delta H^0_{f,comp}$ of these samples are calculated from equation (3-b) due to the stoichiometry.
§$\Delta H^0_{f,comp}$ of these samples are calculated from equation (3-a) due to the stoichiometry.
¶The composition is presented in atomic percentage.

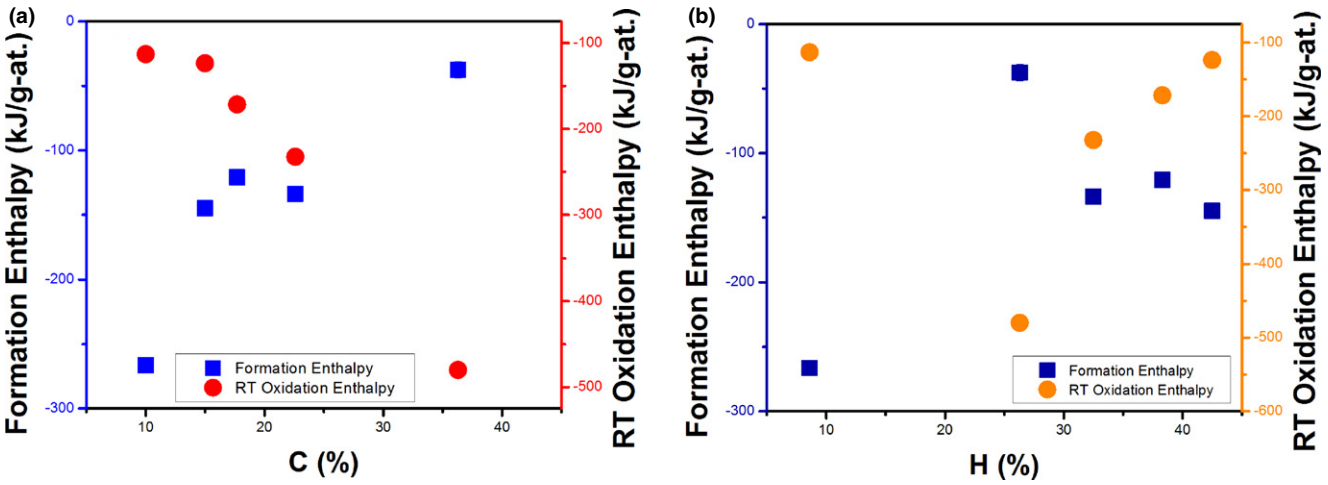

Fig. 5. (a) Oxidation enthalpies at room temperature and formation enthalpies versus the carbon content, (b) Oxidation enthalpies at room temperature and formation enthalpies versus the hydrogen content.

derived ceramics.[28] However, in the work done by Varga *et al.*[12] and Mera *et al.*[26], it was suggested that the mixed bonds at the interface between the free carbon sheet and the nanoscale amorphous region played a role in stabilizing the hydrogen-free polymer-derived ceramics. The films studied here, although having similar composition, in terms of Si, C, and O content to the polymer-derived ceramics, have quite different structures and no evidence for mixed bonds. Nevertheless, their energetic stability is equal to or greater than that of the PDCs.

To observe the hydrogen effect on stabilization, the enthalpies are also plotted against the hydrogen concentration. In Fig. 5(b), the formation enthalpies become more exothermic when hydrogen content increases, but there is one exception with extraordinary stability with hydrogen content at 8.6 at.% (Sample #5). To explain this observation, the molar ratios of the constituent elements (C and H) are calculated against silicon contents. The carbon/silicon ratio is almost same for all samples, except for sample #5. Hence, these five samples can be divided into two categories—one is comprised of samples with high carbon content and the other is #5, with lower carbon content. Since the carbon content makes the main contribution to the oxidation enthalpy and to the destabilization effect, only four high-carbon samples are considered here to observe the hydrogen effect. The formation enthalpies from elements become more exothermic as hydrogen content increases, indicating higher thermodynamic stability at higher hydrogen content.

The thermodynamic stability brought by hydrogen may originate because hydrogen atoms form functional groups, mainly–CH_3, on the surface, thus saturating surface bonding and eliminating defects such as dangling bonds. This conclusion can also be supported by considering the enthalpy of oxidation from the scission and formation of chemical bonds. The estimated oxidation enthalpy of carbon in the free carbon configuration, bridging bond and in methyl group depicted in Scheme 1, are −1606.42, −1372.21, and −877.42 kJ/mol, respectively. (The bond energy information is obtained from Ref. [49]) This clearly shows that the conversion of carbon into methyl group configurations by incorporating hydrogen atoms brings the system more thermodynamic stability.

The FTIR spectra show that, despite smaller carbon content in sample #1, its –CH_x signal is the strongest among all samples, while its Si–C signal is very weak. It is reasonable to surmise that the incorporation of hydrogen into the system causes the formation of more –CH_x functional groups and less incorporation of carbon in the matrix. These surface functional groups greatly increase the thermodynamic stability This conclusion is consistent with the previous work by Tavakoli *et al.*[28] Das *et al.* also demonstrated good thermal stability of SiOCH films by FTIR spectroscopy.[47] It was reported that upon annealing to 600°C, there is no detectable structural change from the FTIR spectroscopy. However, above 600°C, the decomposition of SiOCH films started in terms of breaking H-terminated bonds, followed by microstructural change and segregation of carbon. Braginsky *et al.*[50] reported similar results using Monte Carlo simulation and suggesting that the reaction of O atoms with –CH_3 groups is not the determining step during the oxidation, but the surface recombination and diffusion of the oxygen atoms is the critical step. Therefore, denser structures have better oxidation resistance. However, Narisawa *et al.* reported different results, claiming that the incorporation of hydrogen has an adverse influence on the oxidation behavior of SiOCH polymer-derived ceramics.[13] There could be many concerns about this conclusion; for instance, the surface area difference in materials may result in quite different oxidation behavior. One should also note that, from a kinetic perspective, the observed thermal stability (i.e., persistence to high temperature under a given set of conditions) can be quite different from the thermodynamic stability.

Although the incorporation of hydrogen in the system surely brings higher thermodynamic stability, the question of why these a-SiOCH films tend to lose hydrogen during the manufacturing process still remains unresolved. In many cases, hydrogen and organics are removed during exposure to aggressive wet chemical and plasma-based cleans and etches where the a-SiOCH material is exposed to large concentrations of atomic oxygen, hydrogen, and other energized radicals.[20,25] Hydrogen/organic loss via these mechanisms leads to the creation of numerous unpassivated bonds and

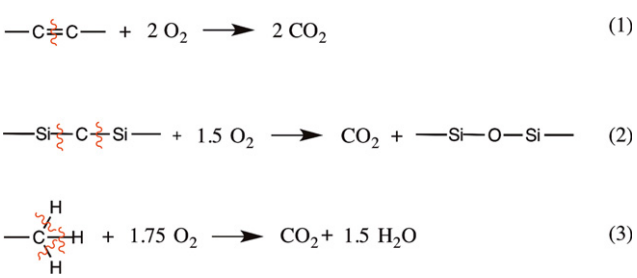

Scheme 1. Oxidation reaction for different configurations of carbon in the structure.

defects that rearrange on thermal annealing to lower their free energy. In other cases, hydrogen/organic loss can start to occur once the SiOCH material is heated above its deposition or curing temperature (typically 200°C).[21,22] To explain this, the entropy related to the release of hydrogen gas must be considered. The reaction related to this process is:

$$\mathrm{Si}_a\mathrm{O}_b\mathrm{C}_c\mathrm{H}_d\ (\text{amorphous solid,25°C}) \rightarrow \mathrm{Si}_a\mathrm{O}_b\mathrm{C}_c\ (\text{amorphous solid,25°C}) + \frac{d}{2}\mathrm{H}_2\ (\text{gas,25°C}) \quad (4)$$

The enthalpy of formation from SiO_2, C, SiC, and H_2 generally becomes less negative as the hydrogen content decreases. Comparing our data with that of Varga et al.[12] for hydrogen-free PDCs, the enthalpies of reaction (4) vary with respect to different a-SiOCH materials, but are mainly positive. Assuming the entropies of the solid phases are similar, the entropy of reaction (4) is dominated by the entropy of hydrogen gas and is on the order of 100 $J\cdot(K)^{-1}$ per mol of H_2 gas produced. Thus, as temperature increases, entropy drives the reaction to the right, as the small positive enthalpy of reaction is not enough to offset the entropy term. Since hydrogen is then released into an essentially H_2-free atmosphere, equilibrium is not attained, and the rate of hydrogen loss is governed by kinetic factors. The important point is that although hydrogen does stabilize the films energetically to some extent, this stabilization is not enough to prevent entropy-driven hydrogen loss upon heating.

IV. Conclusion

Amorphous SiOCH films exhibit significant thermodynamic stability. The incorporation of hydrogen brings more negative enthalpies of formation caused by the surface functional groups, such as $–CH_3$. To achieve better thermodynamic stability, and probably better thermal persistence, several strategies can be employed, such as reducing the free carbon content, incorporating more hydrogen, or maximizing functional groups. However, the energetic stabilization by hydrogen incorporation is not enough to offset the large entropy gain upon hydrogen release, so hydrogen loss during processing at higher temperatures must be managed by kinetic rather than thermodynamic strategies.

Acknowledgment

Synthesis and partial characterization of the samples was performed at the Logic Technology Development facility of the Intel Corporation in Hillsboro, Oregon, USA. Partial characterization and calorimetric measurements were performed at the Peter A. Rock Thermochemistry Laboratory at the University of California, Davis, USA, supported by the Intel Corporation. Salary support was provided as part of the Fluid Interface Reactions, Structures & Transport, an Energy Frontier Research Center funded by the U.S. Department of Energy, Office of Science, Office of Basic Energy Sciences under Award Number 4000134953.

References

[1]F. Danes, E. Saint-Aman, and L. Coudurier, "The Si–C–O System," *J. Mater. Sci.*, **28** [2] 489–95 (1993).

[2]M. Nagamori, I. Malinsky, and A. Claveau, "Thermodynamics of the Si–C–O System for the Production of Silicon Carbide and Metallic Silicon," *MTB*, **17** [3] 503–14 (1986).

[3]L. M. Han, J.-S. Pan, S.-M. Chen, N. Balasubramanian, J. Shi, et al., "Characterization of Carbon-Doped SiO_2 Low *k* Thin Films: Preparation by Plasma-Enhanced Chemical Vapor Deposition from Tetramethylsilane," *J. Electrochem. Soc.*, **148** [7] F148–53 (2001).

[4]S. Gallis, V. Nikas, E. Eisenbraun, M. Huang, and A. E. Kaloyeros, "On the Effects of Thermal Treatment on the Composition, Structure, Morphology, and Optical Properties of Hydrogenated Amorphous Silicon Oxycarbide," *J. Mater. Res.*, **24** [08] 2561–73 (2009).

[5]C. Moysan, R. Riedel, R. Harshe, T. Rouxel, and F. Augereau, "Mechanical Characterization of a Polysiloxane-Derived SiOC Glass," *J. Eur. Ceram. Soc.*, **27** [1] 397–403 (2007).

[6]P. Du, X. Wang, I. K. Lin, and X. Zhang, "Effects of Composition and Thermal Annealing on the Mechanical Properties of Silicon Oxycarbide Films," *Sens. Actuat. A Phys.*, **176**, 90–8 (2012).

[7]M. Nastasi, Q. Su, L. Price, J. A. Colón Santana, T. Chen, et al., "Superior Radiation Tolerant Materials: Amorphous Silicon Oxycarbide," *J. Nucl. Mater.*, **461**, 200–5 (2015).

[8]R. Zhuo, P. Colombo, C. Pantano, and E. A. Vogler, "Silicon Oxycarbide Glasses for Blood-Contact Applications," *Acta Biomater.*, **1** [5] 583–9 (2005).

[9]N. Suyal, T. Krajewski, and M. Mennig, "Microstructural and Dielectric Characterization of Sol–Gel Derived Silicon Oxycarbide Glass Sheets," *J. Sol-Gel. Sci. Technol.*, **14** [1] 113–23 (1999).

[10]T. Rouxel, G. Massouras, and G.-D. Sorarù, "High Temperature Behavior of a Gel-Derived SiOC Glass: Elasticity and Viscosity," *J. Sol-Gel. Sci. Technol.*, **14** [1] 87–94 (1999).

[11]T. Rouxel, J.-C. Sanglebœuf, J.-P. Guin, V. Keryvin, and G.-D. Soraru, "Surface Damage Resistance of Gel-Derived Oxycarbide Glasses: Hardness, Toughness, and Scratchability," *J. Am. Ceram. Soc.*, **84** [10] 2220–4 (2001).

[12]T. Varga, A. Navrotsky, J. L. Moats, R. M. Morcos, F. Poli, et al., "Thermodynamically Stable $Si_xO_yC_z$ Polymer-Like Amorphous Ceramics," *J. Am. Ceram. Soc.*, **90** [10] 3213–9 (2007).

[13]M. Narisawa, K. Terauds, R. Raj, Y. Kawamoto, T. Matsui, and A. Iwase, "Oxidation Process of White Si–O–C(–H) Ceramics with Various Hydrogen Contents," *Scripta Mater.*, **69** [8] 602–5 (2013).

[14]A. Grill, S. M. Gates, T. E. Ryan, S. V. Nguyen, and D. Priyadarshini, "Progress in the Development and Understanding of Advanced Low k and Ultralow k Dielectrics for Very Large-Scale Integrated Interconnects—State of the Art," *Appl. Phys. Rev.*, **1** [1] 011306, 17pp (2014).

[15]S. Gallis, V. Nikas, M. Huang, E. Eisenbraun, and A. E. Kaloyeros, "Comparative Study of the Effects of Thermal Treatment on the Optical Properties of Hydrogenated Amorphous Silicon Oxycarbide," *J. Appl. Phys.*, **102** [2] 024302, 9pp (2007).

[16]A. Grill and V. Patel, "Ultralow-k Dielectrics Prepared by Plasma-Enhanced Chemical Vapor Deposition," *Appl. Phys. Lett.*, **79** [6] 803–5 (2001).

[17]A. M. Wrobel, P. Uznanski, A. Walkiewicz-Pietrzykowska, B. Glebocki, and E. Bryszewska, "Silicon Oxycarbide Thin Films by Remote Microwave Hydrogen Plasma CVD Using a Tetramethyldisiloxane Precursor," *Chem. Vap. Deposition*, **21** [4–5–6] 88–93 (2015).

[18]V. Rouessac, L. Favennec, B. Rémiat, V. Jousseaume, G. Passemard, and J. Durand, "Precursor Chemistry for ULK CVD," *Microelectron. Eng.*, **82** [3–4] 333–40 (2005).

[19]K. Maex, M. R. Baklanov, D. Shamiryan, F. lacopi, S. H. Brongersma, and Z. S. Yanovitskaya, "Low Dielectric Constant Materials for Microelectronics," *J. Appl. Phys.*, **93** [11] 8793–841 (2003).

[20]M. R. Baklanov, J.-F. de Marneffe, D. Shamiryan, A. M. Urbanowicz, H. Shi, et al., "Plasma Processing of Low-k Dielectrics," *J. Appl. Phys.*, **113** [4] 041101, 41pp (2013).

[21]T. Furusawa, D. Ryuzaki, R. Yoneyama, Y. Homma, and K. Hinode, "Heat and Moisture Resistance of Siloxane-Based Low-Dielectric-Constant Materials," *J. Electrochem. Soc.*, **148** [9] F175–9 (2001).

[22]M. G. Albrecht and C. Blanchette, "Materials Issues with Thin Film Hydrogen Silsesquioxane Low K Dielectrics," *J. Electrochem. Soc.*, **145** [11] 4019–25 (1998).

[23]A. Grill, "PECVD Low and Ultralow Dielectric Constant Materials: From Invention and Research to Products," *J. Vac. Sci. Technol., B*, **34** [2] 020801, 9pp (2016).

[24]F. Iacopi, S. H. Brongersma, B. Vandevelde, M. O'Toole, D. Degryse, et al., "Challenges for Structural Stability of Ultra-Low-k-Based Interconnects," *Microelectron. Eng.*, **75** [1] 54–62 (2004).

[25]D. Moore, R. Carter, H. Cui, P. Burke, P. McGrath, et al., "Process Integration Compatibility of Low-k and Ultra-Low-k Dielectrics," *J. Vacuum Sci. Technol. B*, **23** [1] 332–5 (2005).

[26]G. Mera, A. Navrotsky, S. Sen, H.-J. Kleebe, and R. Riedel, "Polymer-Derived SiCN and SiOC Ceramics—Structure and Energetics at the Nanoscale," *J. Mater. Chem. A*, **1** [12] 3826–36 (2013).

[27]X. Wang, J. Wu, Y. Li, C. Zhou, and C. Xu, "Pyrolysis Kinetics and Pathway of Polysiloxane Conversion to an Amorphous SiOC Ceramic," *J. Therm. Anal. Calorim.*, **115** [1] 55–62 (2014).

[28]A. H. Tavakoli, M. M. Armentrout, M. Narisawa, S. Sen, and A. Navrotsky, "White Si–O–C Ceramic: Structure and Thermodynamic Stability," *J. Am. Ceram. Soc.*, **98** [1] 242–6 (2015).

[29]A. H. Tavakoli, M. M. Armentrout, S. Sen, and A. Navrotsky, "Hydrogenated Si–O–C Nanoparticles: Synthesis, Structure, and Thermodynamic Stability," *J. Mater. Res.*, **30** [02] 295–303 (2015).

[30]S. W. King, M. French, M. Jaehnig, M. Kuhn, and B. French, "X-ray Photoelectron Spectroscopy Investigation of the Schottky Barrier at Low-k a-SiO(C):H/Cu Interfaces," *Appl. Phys. Lett.*, **99** [20] 202903, 3pp (2011).

[31]Y. Matsuda, N. Kim, S. W. King, J. Bielefeld, J. F. Stebbins, and R. H. Dauskardt, "Tunable Plasticity in Amorphous Silicon Carbide Films," *ACS Appl. Mater. Interfaces*, **5** [16] 7950–5 (2013).

[32]S. Bailey, E. Mays, D. J. Michalak, R. Chebiam, S. King, and R. Sooryakumar, "Mechanical Properties of High Porosity Low-k Dielectric Nano-Films Determined by Brillouin Light Scattering," *J. Phys. D Appl. Phys.*, **46** [4] 045308, 7pp (2013).

[33]S. W. King, M. French, J. Bielefeld, and W. A. Lanford, "Fourier Transform Infrared Spectroscopy Investigation of Chemical Bonding in Low-k a-SiC:H Thin Films," *J. Non-Cryst. Solids*, **357** [15] 2970–83 (2011).

[34]F. Doniat, C. Anderson, C. Dussarrat, J. McAndrew, R. Opila, et al., "Development of Low-k Precursors for Next Generation IC Manufacturing," *Microelectron. Eng.*, **9**, 34–7 (2012).

[35]M. J. Cordill, F. D. Fischer, F. G. Rammerstorfer, and G. Dehm, "Adhesion Energies of Cr Thin Films on Polyimide Determined from Buckling: Experiment and Model," *Acta Mater.*, **58** [16] 5520–31 (2010).
[36]S. W. King and M. Milosevic, "A Method to Extract Absorption Coefficient of Thin Films from Transmission Spectra of the Films on Thick Substrates," *J. Appl. Phys.*, **111** [7] 073109, 9pp (2012).
[37]M. Milosevic and S. W. King, "Analysis of Low-k Dielectric Thin Films on Thick Substrates by Transmission FTIR Spectroscopy," *ECS J. Solid State Sci. Technol.*, **4** [1] N3146–52 (2015).
[38]A. Navrotsky, "Progress and New Directions in High Temperature Calorimetry," *Phys. Chem. Miner.*, **2** [12] 89–104 (1977).
[39]A. Navrotsky, "Progress and New Directions in High Temperature Calorimetry Revisited," *Phys. Chem. Miner.*, **24** [3] 222–41 (1997).
[40]A. Navrotsky, "Progress and New Directions in Calorimetry: A 2014 Perspective," *J. Am. Ceram. Soc.*, **97** [11] 3349–59 (2014).
[41]S. M. Gates, D. A. Neumayer, M. H. Sherwood, A. Grill, X. Wang, and M. Sankarapandian, "Preparation and Structure of Porous Dielectrics by Plasma Enhanced Chemical Vapor Deposition," *J. Appl. Phys.*, **101** [9] 094103, 8pp (2007).
[42]G. Lucovsky, "Chemical Effects on the Frequencies of Si-H Vibrations in Amorphous Solids," *Solid State Commun.*, **29** [8] 571–6 (1979).
[43]E. Gat, M. A. El Khakani, M. Chaker, A. Jean, S. Boily, et al., "A Study of the Effect of Composition on the Microstructural Evolution of a–Si_xC_{1-x}: H PECVD Films: IR Absorption and XPS Characterizations," *J. Mater. Res.*, **7** [09] 2478–87 (1992).
[44]A. Grill and D. A. Neumayer, "Structure of Low Dielectric Constant to Extreme Low Dielectric Constant SiCOH Films: Fourier Transform Infrared Spectroscopy Characterization," *J. Appl. Phys.*, **94** [10] 6697–707 (2003).
[45]A. Saha, R. Raj, and D. L. Williamson, "A Model for the Nanodomains in Polymer-Derived SiCO," *J. Am. Ceram. Soc.*, **89** [7] 2188–95 (2006).
[46]L. Yu and R. Raj, "On the Thermodynamically Stable Amorphous Phase of Polymer-Derived Silicon Oxycarbide," *Sci. Rep.*, **5**, 14550, 13pp (2015).
[47]G. Das, G. Mariotto, and A. Quaranta, "Vibrational Spectroscopy Characterization of Low-Dielectric Constant SiOC:H Films Prepared by PECVD Technique," *Mater. Sci. Semicond. Process.*, **7** [4–6] 295–300 (2004).
[48]P.-Y. Mabboux and K. K. Gleason, "Chemical Bonding Structure of Low Dielectric Constant Si:O:C:H Films Characterized by Solid-State NMR," *J. Electrochem. Soc.*, **152** [1] F7–13 (2005).
[49]J. E. Huheey, E. A. Keiter, R. L. Keiter, and O. K. Medhi, *Inorganic Chemistry: Principles of Structure and Reactivity*. Pearson Education, New York, NY, 2006.
[50]O. V. Braginsky, A. S. Kovalev, D. V. Lopaev, E. M. Malykhin, Y. A. Mankelevich, et al., "The Mechanism of Low-k SiOCH Film Modification by Oxygen Atoms," *J. Appl. Phys.*, **108** [7] 073303, 10pp (2010).
[51]C. W. Bale, P. Chartrand, S. A. Degterov, G. Eriksson, K. Hack, et al., "FactSage Thermochemical Software and Databases," *CALPHAD*, **26** [2] 189–228 (2002).
[52]A. H. Tavakoli, J. A. Golczewski, J. Bill, and A. Navrotsky, "Effect of Boron on the Thermodynamic Stability of Amorphous Polymer-Derived Si(B)CN Ceramics"; *Acta Mater.*, **60** [11] 4514–22 (2012).
[53]R. A. Robie and B. S. Hemingway, "Thermodynamic Properties of Minerals and Related Substances at 298.15 K and 1 bar (10^5 Pascals) Pressure and at Higher Temperatures," *Bulletin*, No. 2131, USGPO, For sale by US Geological Survey, Information Services, Washington, DC, 1995.
[54]Z. Zhou and A. Navrotsky, "Thermochemistry of the Y_2O_3–BaO–Cu–O System," *J. Mater. Res.*, **7** [11] 2920–35 (1992).
[55]M. W. Chase; S National Institute of andTechnology, *NIST-JANAF Thermochemical Tables*. American Chemical Society; American Institute of Physics for the National Institute of Standards and Technology, [Washington, D.C.]; Woodbury, New York, 1998. □

Appendix I

Table AI. Thermochemical Cycles for Low-*k* a-SiOCH Materials

Reaction	Enthalpy (ΔH)
a: Enthalpy of oxidation (ΔH^0_{ox}) at 25°C	
(1) $Si_aO_bC_cH_d$ (solid, 25°C) + $\left(a+c+\frac{d}{4}-\frac{b}{2}\right)$ O_2 (gas, 802°C) → a SiO_2 (cristobalite, 802°C) + c CO_2 (gas, 802°C) + $\frac{d}{2}$ H_2O (gas, 802°C)	$\Delta H_1 = \Delta H_{ds}$ [kJ·(g·at.)$^{-1}$]
(2) SiO_2 (cristobalite, 25°C) → SiO_2 (cristobalite, 802°C)	ΔH_2 = 50.1 kJ/mol[†,51]
(3) H_2O (liquid, 25°C) → H_2O (gas, 802°C)	ΔH_3 = 73.1 kJ/mol[52]
(4) O_2 (gas, 25°C) → O_2 (gas, 802°C)	ΔH_4 = 25.3 kJ/mol[51]
(5) CO_2 (gas, 25°C) → CO_2 (gas, 802°C)	ΔH_5 = 37.5 kJ/mol[51]
$Si_aO_bC_cH_d$ (solid, 25°C) + $\left(a+c+\frac{d}{4}-\frac{b}{2}\right)$ O_2 (gas, 25°C) → a SiO_2(cristobal, 25°C) +c CO_2 (gas, 25°C) + $\frac{d}{2}$ H_2O (liquid, 25°C)	$\Delta H^0_{ox} = \Delta H_1 - a\,\Delta H_2 - \frac{d}{2}\Delta H_3 + \left(a+c+\frac{d}{4}-\frac{b}{2}\right)\Delta H_4 - c\Delta H_5$
b: Enthalpy of formation from the elements $\Delta H^0_{f,elem}$ at 25°C	
(1) $Si_aO_bC_cH_d$ (solid, 25°C) + $\left(a+c+\frac{d}{4}-\frac{b}{2}\right)$ O_2 (gas, 25°C) → a SiO_2(cristobal, 25°C) + c CO_2 (gas, 25°C) + $\frac{d}{2}H_2O$ (liquid, 25°C)	$\Delta H_1 = \Delta H^0_{ox}$ [kJ·(g·at.)$^{-1}$]
(2) Si (solid, 25°C) + O_2 (gas, 25°C) → SiO_2 (cristobalite, 25°C)	$\Delta H_2 = -908.4 \pm 2.1$ kJ/mol[53]
(3) H_2 (gas, 25°C) + 1/2 O_2 (gas, 25°C) → H_2O (liquid, 25°C)	$\Delta H_3 = -285.8 \pm 0.1$ kJ/mol[53]
(4) C (solid, 25°C) + O_2 (gas, 25°C) → CO_2 (gas, 25°C)	$\Delta H_4 = -393.5 \pm 0.1$ kJ/mol[53]
a Si (solid, 25°C) + $\frac{b}{2}O_2$ (gas, 25°C + c C (solid, 25°C) + $\frac{d}{2}$ H_2 (gas, 25°C) → $Si_aO_bC_cH_d$ (solid, 25°C)	$\Delta H^0_{f,elem} = -\Delta H_1 + a\Delta H_2 + \frac{d}{2}\Delta H_3 + c\Delta H_4$
c: Enthalpy of formation from the components $\Delta H^0_{f,comp}$ at 25°C (Version 1)	
(1) a Si (solid, 25°C) + $\frac{b}{2}O_2$ (gas, 25°C) + c C (solid, 25°C) +$\frac{d}{2}$ H_2 (gas, 25°C) → $Si_aO_bC_cH_d$ (solid, 25°C)	$\Delta H_1 = \Delta H^0_{f,elem}$ [kJ·(g·at.)$^{-1}$]
(2) Si (solid, 25°C) + C (solid, 25°C) → SiC (solid, 25°C)	$\Delta H_2 = -73.2 \pm 6.3$ kJ/mol[‡,51]
(3) Si (solid, 25°C) + O_2 (gas, 25°C) → SiO_2 (cristobalite, 25°C)	$\Delta H_3 = -908.4 \pm 2.1$ kJ/mol[53]
$\left(a-\frac{b}{2}\right)$ SiC (solid, 25°C) + $\frac{b}{2}$ SiO_2 (cristobalite, 25°C) + $\left(c-a+\frac{b}{2}\right)$ C (solid, 25°C) + $\frac{d}{2}$ H_2 (gas, 25°C) → $Si_aO_bC_cH_d$ (solid, 25°C)	$\Delta H^0_{f,comp} = \Delta H_1 - \left(a-\frac{b}{2}\right)\Delta H_2 - \frac{b}{2}\Delta H_3$
d: Enthalpy of formation from the components $\Delta H^0_{f,comp}$ at 25°C (Version 2)	
(1) a Si (solid, 25°C) + $\frac{b}{2}O_2$ (gas, 25°C) + c C (solid, 25°C) + $\frac{d}{2}$ H_2 (gas, 25°C) → $Si_aO_bC_cH_d$ (solid, 25°C)	$\Delta H_1 = \Delta H^0_{f,elem}$ [kJ·(g·at.)$^{-1}$]
(2) Si (solid, 25°C) + C (solid, 25°C) → SiC (solid, 25°C)	$\Delta H_2 = -73.2 \pm 6.3$ kJ/mol[51]
(3) Si (solid, 25°C) + O_2 (gas, 25°C) → SiO_2 (cristobalite, 25°C)	$\Delta H_3 = -908.4 \pm 2.1$ kJ/mol[53]
c SiC (solid, 25°C) + $\frac{b}{2}$ SiO_2 (cristobalite, 25°C) + $\left(a-c-\frac{b}{2}\right)$Si (solid, 25°C) + $\frac{d}{2}$ H_2 (gas, 25°C) → $Si_aO_bC_cH_d$ (solid, 25°C)	$\Delta H^0_{f,comp} = \Delta H_1 - c\,\Delta H_2 - \frac{b}{2}\,\Delta H_3$

[†]Low cristobalite at 25°C, high cristobalite at 802°C.
[‡]Enthalpy of formation of β-SiC.

Appendix II: Correction for Metallic Copper

For making correction, we assumed that sample is a mechanical mixture of metallic copper and the analyzed film composition. The enthalpy of drop solution for metallic copper is −96.7 kJ/mol, calculated by using the thermocyclein Table AII. When doing experiment, each pellet dropped into the molten solvent is <1.5 mg. Therefore, the heat of dissolution caused by 10 wt% Cu impurity will be

$$\Delta H_{10\%\,\mathrm{Cu}} = -96.7\,\mathrm{kJ/mol} \times \frac{1.5\,\mathrm{mg} \times 10\%}{63.546\,\mathrm{g/mol}} = -2.28 \times 10^{-4}\,\mathrm{kJ}$$

This is so small compared with the heat effect of each dissolution reaction, which is usually larger than 15 J/mol.

Table AII. Thermochemical Cycle for the Enthalpy of Drop Solution of Metallic Copper

Reaction	Enthalpy
Cu (solid, 298K) + 1/2 O_2 (gas, 298K) → CuO (solid, 298K)	$\Delta H_1 = -157.320 \pm 1.255$ kJ/mol[53]
CuO (solid, 298K) → CuO (solid, 977K)	$\Delta H_2 = 67.9 \pm 0.6$ kJ/mol[54]
CuO (solid, 977K) → CuO (solid, 1075K)	$\Delta H_3 = 5.406$ kJ/mol[55]
O_2 (gas, 298K) → O_2 (gas, 1075K)	$\Delta H_4 = 25.3$ kJ/mol[55]
Cu (solid, 298K) + 1/2O_2 (gas,1075K) → CuO (solid, 1075K)	$\Delta H_{ds} = \Delta H_1 - 0.5\,\Delta H_4 + \Delta H_2 + \Delta H_3 = -96.7$ kJ/mol